Influence of the injection of densified polymer suspension on the efficiency of DNAPL displacement in contaminated saturated soils

Amir Alamooti [a,b,c,*], Stéfan Colombano [a], Sagyn Omirbekov [a,b,d], Azita Ahmadi [b], Fabien Lion [a], Hossein Davarzani [a]

[a] BRGM (French Geological Survey), Orléans 45000, France
[b] Institut de Mécanique et Ingénierie de Bordeaux (I2M), Arts et Métiers Institute of Technology, CNRS, Talence 33405, France
[c] ADEME (Agence de la transition écologique), ANGERS, 49004, France
[d] Nazarbayev University, 53 avenue Qabanbay Batyr, Nur-Sultan 010000, Kazakhstan

HIGHLIGHTS

- Polymer densification can improve DNAPL displacement efficiency up to 4 times more.
- Clogging of barite particles in polymer suspension can cause permeability reduction up to 70%.
- Presence of the barite particle results in higher viscosity of the polymer suspension.
- Two-phase model can properly predict the experimental consequences.
- To mimic the polluted site, using an open-system for displacement efficiency analysis is vital.

GRAPHICAL ABSTRACT

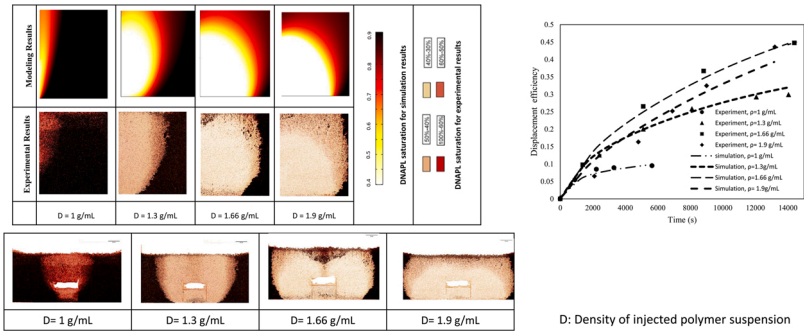

D: Density of injected polymer suspension

ARTICLE INFO

Editor: Feng Xiao

Keywords:
DNAPL
Polymer suspension
Densification
Clogging
Two-phase flow

ABSTRACT

Nowadays the remediation of DNAPL contaminated zones near groundwater has gained great prominence in environmental fields due to the high importance of water resources. In this work, we suggest injecting a densified polymer suspension by adding barite particles to displace DNAPL. To evaluate the efficiency of the densification of polymer suspensions on the displacement of DNAPL, various densities of barite-polymer suspension; lower, equal, and higher than the density of DNAPL were prepared and their rheological behavior was analyzed. Then flow experiments were performed using a decimetric-scale 2D tank. The displacement procedure was monitored with an imaging technique and the production and injection process data were recorded by mass balance interpretation. It was shown that the densification of the polymer suspension could improve the displacement efficiency of DNAPL up to four times. The clogging behavior of barite-polymer suspension was assessed in a 1D column. Generalized Darcy's law and the continuity equation were used to numerically simulate the experimental two-phase flow. To take into account the clogging behavior of the suspension, the transport equation of diluted species was implemented into the model. The simulation results show that the model can properly predicts the experimental consequences.

* Corresponding author at: BRGM (French Geological Survey), Orléans 45000, France.
E-mail address: a.alamooti@brgm.fr (A. Alamooti).

1. Introduction

Dense non-aqueous phase liquids (DNAPLs) such as chlorinated organic compounds have been used for several years for various purposes, including but not limited to the cleaning of fabrics and metal degreasing. The vast consumption of these solvents during the last decades, as well as their inappropriate disposal have caused a plethora of environmental issues. Due to the density of these solvents, they can penetrate through the soil and the groundwater and, consequently, shape discontinuous trapped dense non-aqueous phase liquid (DNAPL) zones (Langwaldt and Puhakka, 2000; Zhang and Smith, 2002). The dissolution of some components of these organic compounds can result in serious groundwater pollution (Roy et al., 2004). Nowadays there are numerous contaminated sites around the world contending with the problems related to the contamination of the groundwater. Displacement and removal of these DNAPLs from their source zones are very challenging and costly (McCarty, 2010). In other words, their high density and interfacial tension as well as their low solubility make the performance of most extraction technologies inefficient (e.g. pump-and-treat-method). The trend in global soil remediation technologies shows that the approach has switched from the pump-and-treat method to more advanced methods, including thermal and chemical enhancement (Colombano et al., 2021, 2020; Stroo et al., 2012).

Among the advanced remediation technologies, invading agents including surfactant, foam and polymer are widely used to displace the residing contaminant (DNAPL as pure phase) from the soil. In the case of the surfactant solution injection, using a high concentration of surfactant (i.e. higher than the critical micelle concentration) can cause the dissolution of the contaminant in the aqueous phase (Johnson et al., 1999). In the event of foam, the foam's stability is one of the challenging issues in design and performance of foam injection (Ardakani et al., 2020; Kilbane et al., 1997; Wang and Mulligan, 2004).

Polymers have been widely used in the petroleum industry as one of the most effective enhanced oil recovery (EOR) technologies for different reservoir types (Alamooti and Malekabadi, 2018; Littmann, 1988; Liu, 2008; Sandiford, 1964). Although the process of DNAPL remediation of contaminated soils is similar to the EOR methods, there are some main differences. Firstly, the porous media in soils are several orders of magnitudes more permeable than reservoir rocks. In addition, the density of DNAPL is higher than the density of water and the location of these contaminants is close to groundwater and due to the high standards of remediation processes, the amount of residual DNAPLs should not exceed several ppm (Kilbane et al., 1997).

To mobilize the trapped ganglia of DNAPL in pore spaces, several forces including the capillary, viscous, gravity, and buoyancy forces are working simultaneously (Dejam et al., 2014; Mashayekhizadeh et al., 2011; Alamooti et al., 2020). The high surface tension of the DNAPLs makes the mobilization process more difficult but in the case of high permeable porous media, the capillary forces are not dominant. To mobilize ganglia of a non-aqueous phase liquid (here DNAPL) the summation of the viscous and gravity forces should be higher than the capillary forces present in polluted soil (Duffield et al., 2003; Jeong, 2005; Li et al., 2007; Pennell et al., 1996). In general, polymers are used to increase the viscous forces to improve the displacement of DNAPL by reducing the instabilities in the invading phase in porous media. Martel et al. (2004) used a polymer solution before and after a micellar solution (composed of a surfactant (12% Hostapur SAS from Clariant), an alcohol (12% *n*-butanol) and two solvents (19% D-limonene; 5% toluene)) to enhance the displacement efficiency of DNAPL. They injected polymer as a preflush slug to limit the mobility of the washing solution and avoid the adsorption of surfactant on the solids, and they injected it as post-flush slug to push out the washing solution of porous media. They found that on the one hand using reduced velocity improved the dissolution of the micellar solution by increasing the contact time and on the other hand, it caused less mobilization of DNAPL due to a decrease in capillary number. They also showed that polymer solution (xanthan gum) can positively improve the front stability. Martel et al. (1998) used the xanthan polymer solution for mobility control during the soil remediation of NAPL in a multilayer system, and they found that the injection of a polymer solution after the surfactant increases the mobility of the surfactant in low permeable zones and decreases it in high permeable zones. Silva et al. (2013) used modeling to simulate the flow of the polymer-improved aquifer remediation. They showed that by using a biopolymer the sweep efficiency was improved more than 70%. Smith et al. (2008) illustrated that the polymer-improved remediation technique (xanthan gum and potassium permanganate) can be used as a robust technology for the displacement of contaminants including PCE.

Miller et al. (2000) introduced a density-motivated mobilization approach for the remediation of DNAPL contaminated soils. They elucidated the idea of modifying the balances between the capillary and buoyancy forces. By means of bench-scale columns and a two-dimensional tank, they performed several displacement experiments where they showed that the efficiency of densified brine solution (using NaI) on displacement of DNAPL can reach up to 70%. They also proved that the densified brine solution can be used as a barrier below the DNAPL pool to prevent the downward movement of the DNPAL when a surfactant solution was used as displacement agent.

From the rheological point of view, polymer solutions are considered as non-Newtonian fluids i.e. their viscosity is a function of shear rate. For the study of fluid flow in porous media, to link the shear rate at bulk scale and fluid velocity in porous media (Darcy velocity) the physical parameters of porous media including permeability, porosity, and tortuosity should be considered (Darby et al., 2017; Omirbekov et al., 2020). For the case of biopolymers such as xanthan and carboxymethyl cellulose (CMC), a shear thinning behavior is observed (Benchabane and Bekkour, 2008; Zhong et al., 2013).

In the case of chlorinated solvents, as they are much denser than water and mainly isolated near the groundwater resources, if a lighter fluid is injected to remediate the contaminated soil, buoyancy forces work against the displacement. Although polymer solutions can provide higher viscous forces, they are lighter than DNAPL and the gravity forces can influence the displacement efficiency of DNAPLs.

Despite numerous studies carried out to evaluate the performance of polymer solutions injection on the displacement of the DNAPLs, the question of how to handle the gravity forces in an open system (without no flow boundaries) of the contaminated soil using a polymer solution is not well addressed in the literature. Furthermore, although the performance of the viscous (e.g. polymer) and dense solutions on the displacement of DNAPL have been individually investigated, the literature is bereft of a study in which a single densified high viscosity mixture has been used to overcome the gravity and capillary forces at the same time. Although using only a polymer solution with higher injection rates can improve the viscous forces, but it can result in viscous fingering and soil push up. Therefore, the novelty of this work is the introduction of a new remediation technology in which a densified polymer suspension has been injected to overcome both the gravity and capillary forces. The injection of dense polymers will therefore allow forcing the polymer to remain at the bottom of the aquifer to better displace the DNAPL. To achieve this goal, we analyzed the performance of a densified polymer suspension on the displacement of DNAPL from contaminated soils where gravity forces are working against the sweeping process. Barite ($BaSO_4$) particles were added to the CMC biopolymer to increase the density (Bern et al., 1996; Hanson et al., 1990) of the polymer suspension and to evaluate the permeability reduction in the displaced zone. Barite has very low solubility in water and is essentially considered nontoxic (Schulz et al., 2018). Also, it is normally ingested by patients who are going to do some X-ray tests on their digestive system (Merian et al., 2004). The main achievement of this study is to introduce densified polymer suspension for the improvement of the displacement efficiency of DNAPL. In addition, it gives insight on not only the application of densified polymer suspension on the displacement of DNAPL but also the role of boundaries on its

performance. In this work, the experimental results on rheological behavior of the densified polymer suspension are provided and then the performance of the densification of the polymer suspension on displacement efficiency of DNAPL is discussed. The role of clogging of suspended particles on the transport of polymer suspension is analyzed. To have better understanding of the displacement process of DNAPL, the two-phase flow was simulated by means of the continuity and Darcy equations (Bear, 2013). The general advection-dispersion-reaction equation was used for the transport of barite and polymer in porous media (O'Carroll et al., 2013).

2. Material and methods (experimental and numerical)

In this section, first the 1D column and 2D tank experimental setups and procedures are explained. Then the method of image interpretation is presented. Finally, the governing equations are given and the numerical simulation method is described. The properties of experimental materials including the contaminant (DNAPL), barite-polymer suspension, soil physics as well as the suspension preparation are discussed in supplementary material part A.1.

2.1. 1D column experiments

To measure the permeability and the porosity of sandpacks with the grain size between 0.6 and 0.8 mm and further analyze the clogging process of barite-polymer suspension, one-dimensional calibrated glass columns were used. The radius and length of the one-dimensional column were 4 cm and 30 cm, respectively.

These experiments were carried out to study the deposition process of barite particles during the barite-polymer suspension injection through the porous media. In this regard, a one-dimensional column was filled with the same sand as the 2D tank (size between 0.6 and 0.8 mm) and fully saturated with water. The permeability and the porosity of the packed columns were first determined. Next, the barite-polymer suspensions were individually injected at a fixed injection rate of 1 mL/min into the fully water saturated column and the density of the effluents (each 4 mL) was monitored. The experiments were continued to reach the steady state condition by monitoring the pressure gradient. In the end, the columns were flushed at the same injection rate for 24 h with water to displace the floating barite particles inside, and then the reduced permeability and porosity were determined. The schematic of the experimental setup used for barite-polymer suspension injection in 1D columns is shown in Fig. 1.

2.2. 2D tank experiments

For the DNAPL displacement experiments, a two-dimensional tank with the size of 50 cm length× 30 cm height× 2 cm width was used (Fig. 2). The front and back of the tank were made of glass to allow the imaging. The tank is filled up to 28 cm with sand of the grain size between 0.6 and 0.8 mm. To inject the suspension uniformly into the porous media a central zone near the injection point (central bottom zone of the tank) is constituted of sandpacks with different permeabilities to represent the injecting well. To fill the 2D tank with sand while injecting water, the central part near the injection point of barite-polymer suspension was separated using two barrier plates (2 cm × 30 cm). Then the sand of the grain size between 0.6 and 0.8 mm was packed on two lateral sides of tank. Then the coarser sand was packed in central part while the barrier plates were pulled out gradually. When the level of the sandpacks reached a 6 cm height in the entire 2D tank, the coarser sand was covered by 3 cm height of fine sand in the central part. While the sand of the grain size between 0.6 and 0.8 mm was packed everywhere in the 2D tank, the two barrier plates were completely pulled out of the 2D tank. This configuration is close to the field where the polymer is injected using a vertical well into the contaminated zone. Two lateral counter channels (cavities) with the size of 2 cm × 2 cm × 30 cm located at the two sides of the tank were used to regulate the fluid levels during the experiment. The schematic of the tank and the different permeability zones inside are depicted in Fig. 2.

These experiments were performed to investigate the efficiency of the injection of a barite-polymer suspension on the displacement of DNAPL inside porous media. To keep the water level constant during the experiment, demineralized water was recirculated in the tank using two Watson Marlow peristaltic pumps. After the completion of the packing of the sand within the water phase, DNAPL was injected from the three ports (d= 0.16 cm) located at the bottom of the tank at the injection rate of 2 mL/min, to reach the height of 20 cm. Then, the barite-polymer suspension was injected from the bottom center of the tank at the constant injection rate of 1.7 mL/min equivalent to an injection velocity of 1 m/day using a peristaltic pump. Using another peristaltic pump, produced DNAPL was pumped out from the cavities and the level of DNAPL inside the cavities was kept constant during the experiments. By means of a mass scale (Sartorius Cubis MSE8201S-000-D0) the mass of recovered DNAPL was measured and a real-time data acquisition was performed. 2D-images of the tank were recorded regularly during the experiments for further analysis of the evolution of the system, using a digital camera (Nikon® D810 with NIKKOR LENS 105). The schematic of barite-polymer suspension/DNAPL displacement is shown in Fig. 3.

2.3. Suspensions preparation

As the barite particles are almost insoluble in water (Ropp, 2012), the polymer is used, not only to provide a high viscosity but also to cause a stable suspension. In this regard, the role of different polymers on the stability of barite suspension at the same density as the DNAPL ($\rho = 1.66$ g/mL) has been examined.

For this purpose, the efficiency of three different biopolymers including xanthan gum, guar gum, and CMC on the stability of the barite suspension was evaluated. The density of the barite-polymer suspensions was kept at the density of the DNAPL (1.66 g/mL) and the concentration of the polymers was set at 4 g/L. The concentration of polymer was selected in a way to provide sufficient viscous forces to displace the DNAPL in soil but not too high to avoid very high injection pressures. Demineralized and degassed water was used to prepare all the

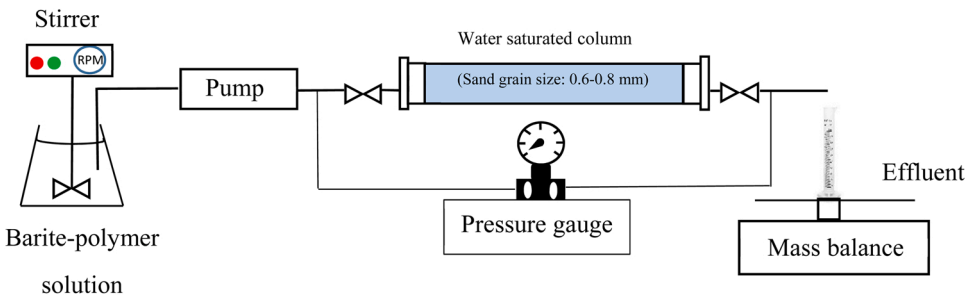

Fig. 1. Schematic of barite-polymer solution injection in 1D column.

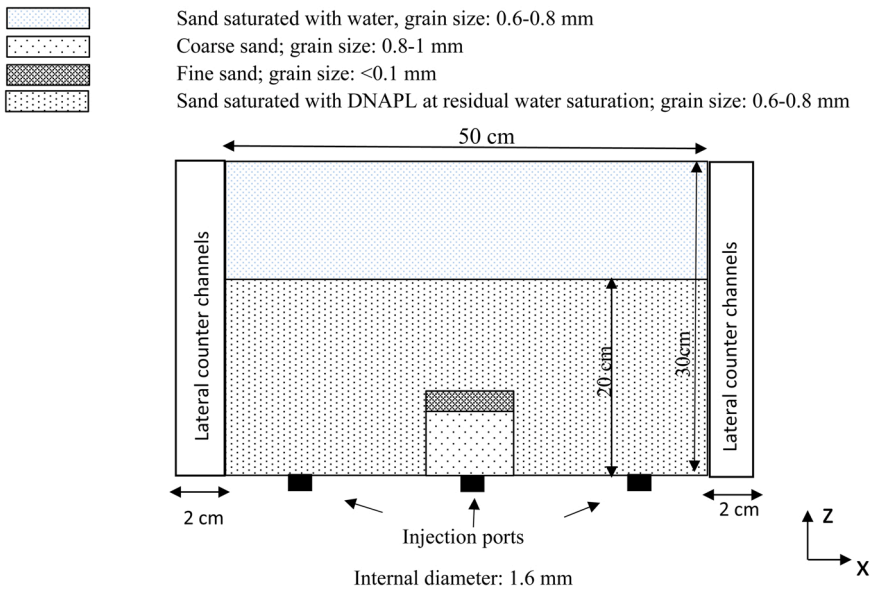

Fig. 2. Schematic of 2D tank (configurations of fluids and sands).

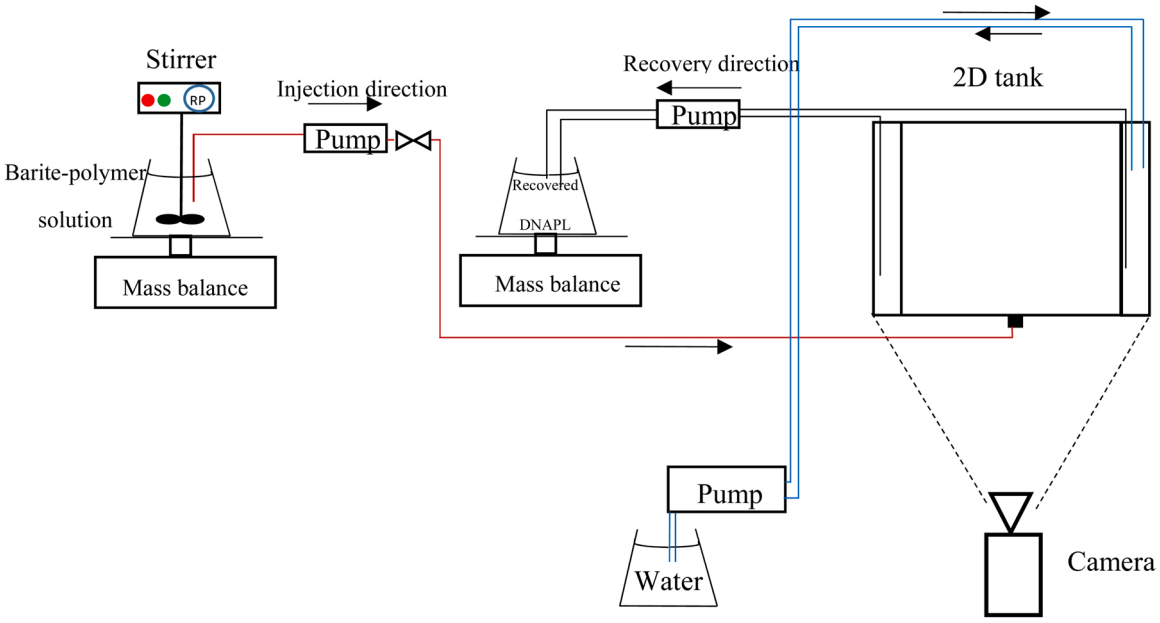

Fig. 3. Schematic of barite-polymer solution-DNAPL displacement experimental setup (2D tank.

suspensions. For the case of polymer solution (without barite particles), polymer powder was added gradually to water, and it was mixed properly using an overhead stirrer (IKA RW14) with 500 RPM for 2 h. For the barite-polymer suspensions, firstly barite particles were added to water while stirring at 200 RPM for 15 min. Then the polymer powder was added very slowly, and the suspension was stirred for 2 h at 500 RPM. Using a graduated cylinder, the decantation process of the barite-polymer suspensions was monitored for 48 h. The results evidenced the sedimentation of a given percentage of the barite particles in the suspension and therefore separation of water from the suspension. When CMC was used as the polymer, 98% of the mixture was kept in the suspension while for xanthan gum and guar gum, this value was 48% and 64% respectively. Therefore, for our study, barite and CMC polymer suspension was chosen to displace the DNAPL inside the soil. For the densities of barite-CMC suspensions of 1.3, 1.66, and 1.9 g/mL, the volume fractions of barite particles inside the suspension were around 8%, 18% and 24%, respectively.

2.4. *Image interpretation*

An image analysis tool is used to describe the displacement process during the 2D tank experiments and to evaluate DNAPL saturation. All the experiments were carried out in a darkroom and the lighting was provided by two light spots (2 ×300 W, Broncolor®). Black and white reflectors were set near the 2D tank to prevent reflections during the photography. A grayscale calibration card was installed on the 2D tank front surface to help regulate the light density for different experiments during image analysis. The lighting differences were adjusted with the 8-grayscale levels. For image interpretation, the area of interest (AOI) was considered almost the same size as the tank glass lateral surface to have a maximum zone of analysis and also to avoid the role of wall shade on the process of the calculation of phases' saturation (Colombano et al., 2021;

Davarzani et al., 2021; Philippe et al., 2020). Next, the size of the pixel area was selected in a way to exclude microscale effect, shadows, and non-uniform lighting effects. To find the relationship between the optical density and DNAPL saturation a calibration curve was used. The optical density of reflected light, O_d, can be expressed as (Flores et al., 2011; Schincariol et al., 1993).

$$O_d = -log\ (\rho_t) \tag{1}$$

$$\rho_t = \frac{I_r}{I_0} \tag{2}$$

where O_d is the optical density of reflected light, ρ_t is the ratio of reflected luminous intensity, I_r and the initial luminous intensity, I_0.

In the next step, the exact optical densities for fully DNAPL-saturated and dry tank (saturations of 1 and 0 respectively), as well as those corresponding to the residual saturations of the wetting and non-wetting phases were determined. With these points, a linear calibration curve has been considered for optical densities and DNAPL saturation (Colombano et al., 2021). To calculate the total DNAPL saturation, the saturation of DNAPL in each pixel was calculated using the average optical density and then for the entire AOI (area of interest) the summation of all saturation was calculated. Indeed, the sum is needed to calibrate the image interpretation vs mass balance data.

2.5. Governing equations

2.5.1. Two-phase non-Newtonian flow in porous media

Natural soil in the contaminated zone below the groundwater level is represented as a non-deformable, uniform and isotropic porous medium containing two incompressible, immiscible phases (aqueous and DNAPL). The continuity equation for each phase can be written as follows (Bear, 2013):

$$\frac{\partial}{\partial t}(\varnothing \rho_i S_i) + \nabla \cdot (\rho_i \boldsymbol{u_i}) = 0 \quad with \quad i = w, \quad nw \tag{3}$$

where the subscripts w and nw denote wetting and non-wetting phases, respectively. $\varnothing$ is the porosity, $\rho_i (kg/m^3)$, S_i and $\boldsymbol{u_i}$ (m/s) are respectively the fluid density, saturation, and Darcy velocity vector for phase i, and t is the time (s). For the momentum equation in porous media the generalized Darcy law is considered:

$$\boldsymbol{u_i} = -\frac{k\ k_{ri}}{\mu_i}(\nabla p_i - \rho_i \boldsymbol{g}) \tag{4}$$

where k (m^2) is the absolute permeability of the isotropic porous medium considered here, k_{ri}, μ_i, and $_{\text{pi}}$ are respectively the relative permeability, viscosity (Pa.s) and the pressure (Pa) of phase i, and $\mathbf{g}$ is the gravity vector. To solve the system of equations for two-phase flow, two other algebraic equations are necessary and are given by:

$$S_w + S_{nw} = 1 \tag{5}$$

$$p_c = p_{nw} - p_w \tag{6}$$

where S_w and S_{nw} are wetting and non-wetting phase saturations. p_c is the capillary pressure (Pa) with p_w and p_{nw}, the wetting and non-wetting phase pressures (Pa), respectively. For the relative permeability and capillary pressure curves we used Brooks and Corey functions (Brooks and Corey, 1964):

$$p_c = p_{th} S_{we}^{\frac{-1}{\lambda}} \tag{7}$$

$$k_{rw} = S_{we}^{\left(3+\frac{2}{\lambda}\right)} \tag{8}$$

$$k_{rnw} = S_{nwe}^{2\left(1-(1-S_{nwe})^{\left(1+\frac{2}{\lambda}\right)}\right)} \tag{9}$$

where p_{th} is the threshold pressure (Pa) and λ is the index of the pore size distribution. S_{we} and S_{nwe} are the effective saturations of wetting and non-wetting phases and are defined as follows:

$$S_{we} = \frac{S_w - S_{wr}}{1 - S_{nwr} - S_{wr}} \tag{10}$$

$$S_{nwe} = \frac{S_{nw} - S_{nwr}}{1 - S_{nwr} - S_{wr}} \tag{11}$$

where, S_{wr} and S_{nwr} are the wetting irreducible and non-wetting residual saturations respectively. As CMC polymer is soluble in water, it is considered as an aqueous phase and is treated as a species transported by water. Due to the non-Newtonian behavior of the barite-polymer suspension, several rheological studies were carried out on the barite-polymer suspension with different Barite concentrations (discussed in results and discussion part). Among various possible models to describe the non-Newtonian behavior of the barite-polymer suspension, the power-law model was found to be the most suitable (Benchabane and Bekkour, 2008):

$$\mu = \kappa \dot{\gamma}^{n-1} \tag{12}$$

where κ is the flow consistency index ($Pa.s^n$), $\dot{\gamma}$ is the shear rate (s^{-1}) and n is the flow behavior index. The values of n less than 1 correspond to a shear-thinning behavior while the values of n more than unity are for shear thickening fluids. The concept of shear rate in porous media, i.e. at the Darcy scale using the Darcy velocity can be expressed as (Darby et al., 2017)

$$\dot{\gamma} = \frac{4\alpha u/\phi}{R_{eq}} \tag{13}$$

where α is the empirical shifting parameter depending on the tortuosity of porous media as well as the bulk rheology of the fluid (Chauveteau and Zaitoun, 1981), and R_{eq} (m) is the average pore throat radius which, using a simple bundle of capillary tubes model, can be estimated as:

$$R_{eq} = \sqrt{\frac{8k}{\phi}} \tag{14}$$

By introducing Eqs. (12)–(14) into Eq. (4) the apparent viscosity term for the aqueous phase can be rewritten as:

$$\mu_w = \alpha\kappa \quad \left(\sqrt{\frac{2k}{\phi}} k_{rw} \left(\nabla p_w - \rho_w \boldsymbol{g}\right)\right)^{\frac{n-1}{n}} \tag{15}$$

2.5.2. Polymer and barite particle transport model

As the barite-polymer has been used to displace DNAPL in porous media, the modeling of the transport of suspended barite particles and polymer in water is considered. A suspension of barite-polymer was injected at a fixed flow rate into a porous medium. Considering the deposition of the suspended barite particles onto the sand grain surfaces, the advection of the barite-polymer in porous media and the hydrodynamic dispersion of the barite particles, the general advection-dispersion-reaction equation for the transport of barite and polymer in porous media can be written as (O'Carroll et al., 2013; Tsakiroglou et al., 2018):

$$\underbrace{\frac{\partial(\varnothing S_w c_i)}{\partial t}}_{Accumulation} - \underbrace{\nabla \cdot (\varnothing S_w \boldsymbol{D} \cdot \nabla c_i)}_{Dispersion} + \underbrace{\boldsymbol{u_w} \cdot \nabla c_i}_{Advection} = R_i + \dot{m} \tag{16}$$

where c_i is the concentration of the i-component (barite or polymer) (kg/

m^3), $\boldsymbol{D}$ is the dispersion tensor, R_i is the reaction term for the *i*-component and $\dot{m}$ is the source term. Hydrodynamic dispersion determines the behavior of components transport in porous media.

The longitudinal and transverse dispersion coefficients are considered and can be expressed as (Auset and Keller, 2004):

$$D_L = D_0 + \propto_L u \tag{17}$$

$$D_T = D_0 + \propto_T u \tag{18}$$

where D_L and D_T are the longitudinal and transverse dispersion coefficients respectively, D_0 is the effective diffusion coefficient (m^2/s) in porous media, $\propto_L$ and $\propto_T$ are the longitudinal and transvers dispersivities, respectively. Since the barite particles have very low solubility in water, physical clogging happens in porous media as a result of suspended particles retention (De Vries, 1972; Vigneswaran and Suazo, 1987). The same transport properties (dispersion tensor, effective diffusion coefficient) are considered for polymer and barite species. Several theoretical and empirical models have been developed to describe the physical clogging process in porous media (Bedrikovetsky et al., 2012; Boek et al., 2012; Yuan and Shapiro, 2011). While empirical models focus on the infiltration rate and particle concentrations in suspension and deposition (Pérez Paricio, 2001), theoretical models debate over the dynamics of the attachment and detachment process. The process of clogging is under the influence of the interaction of several forces including gravity, inertia, electrostatic, and viscous forces (Zamani and Maini, 2009).

Here, we use the transition-deposition model in porous media to simulate the physical clogging in soil (Zheng et al., 2014). The clogging process was coupled with density variations inside the displaced zone and permeability/porosity reduction. According to Eq. (16), the formulation of barite particle transport in porous media can be described as (Zheng et al., 2014):

$$\frac{\partial(\varnothing c_b + c_s)}{\partial t} + \boldsymbol{u}_w \cdot \nabla c_b - \nabla \cdot \left(\varnothing S_w \boldsymbol{D} \cdot \nabla c_b \right) = 0 \tag{19}$$

where c_b is the barite particle concentration in the bulk of suspension (kg/m^3), c_s is the concentration of barite particles deposited on the sand grain surfaces per unit pore volume (kg/m^3). To simulate the process of the clogging caused by barite deposition on the surfaces of the sand grains, the continuity equation was coupled with the transport-deposition equation for barite particles. According to the process of attachment and detachment of particles in porous media, the mechanism of deposition of the suspended barite particles can be described as (Herzig et al., 1970):

$$\frac{\partial c_s}{\partial t} = \theta c_b - \beta c_s \tag{20}$$

where θ is the particle attachment coefficient (s^{-1}) and β is the particle detachment coefficient (s^{-1}). During the injection of barite-polymer suspension the particles of barite can easily be captured by sand grain surfaces, leading to the reduction of pore space (porosity):

$$\varnothing = \varnothing_0 - \frac{c_s}{\rho_b} \tag{21}$$

where $\varnothing_0$ is the initial porosity, ρ_b is the solid barite density (kg/m^3). To correlate the permeability-porosity changes in the displaced zone, the Carman-Kozeny relationship was used (Hommel et al., 2018; Voronov et al., 2010):

$$k = k_0 * CF * \frac{\varnothing^3}{(1-\varnothing)^2} * \frac{(1-\varnothing_0)^2}{\varnothing_0{}^3} \tag{22}$$

where k_0 is the initial absolute permeability, and CF is a correction factor to incorporate the changes in sphericity and diameters of sand particles after deposition of barite particles. The degree of clogging is evaluated using the absolute permeability reduction term as $\frac{(k_0-k)}{k_0}$ (Zheng et al., 2014).

To simulate the system of the partial differential Eqs. (3), (16), and (19) coupled with algebraic Eqs. (5) and (6) in a two-dimensional domain. MUMPS (multifrontal massively parallel sparse direct solver) solver in COMSOL Multiphysics as a finite element solver with a BDF (backward differentiation formula) time stepping was used. The relative tolerance was preset at 0.005 and the absolute scaled tolerance with a factor of 0.1 was considered. The triangular meshing tool of COMSOL with maximum element size of 0.77 cm and minimum element size of 0.0029 cm and a maximum element growth rate of 1.2 was used.

3. Results

Firstly, the rheological behavior of polymer mixture with and without the barite particles was evaluated. Then, the experimental results of the barite particles clogging in the sand is discussed and finally, the results on the efficiency of the barite-polymer suspension on the displacement of the DNAPL is analyzed.

3.1. Rheological behavior of the densified polymer suspension

For the evaluation of the rheological behavior of the barite-CMC suspension the rotational rheometer, Haake Mars 60 was used. To characterize the rheological behavior of the barite-CMC suspension with different densities the variation of the viscosity versus the shear rate in the range of 0.1–100 1/s was analyzed. Fig. 4 shows the viscosity of barite-CMC suspensions for different densities as a function of the shear rate in a log-log scale. It can be seen that the viscosity increases with the density of the mixture. For all polymer mixtures with or without barite particles in the shear rate range used in this study, a shear-thinning behavior can be observed which corresponds to less resistance against the flow at higher shear rates. For the case of CMC solution without barite particles ($\rho = 1$ g/mL), at low shear rate an initial shear thickening behavior can be noted. This increase in viscosity at low shear rate is still controversial. Liu et al. (2007) have attributed this mechanism to "flow induced formation of macromolecular associations". Benchabane and Bekkour (2008) observed this behavior for high concentrations of CMC polymer solution at low shear rate. They reported that one of the most probable reasons for this behavior can be the increase in intermolecular interactions due to the increase in shear rate. In other words, this shear thickening behavior is ascribed to stiffer inner structure due to the formation of entanglements of polymer coils as the shear rate increases.

A power-law model as described earlier (Eq. (12)) was fitted to the rheological behavior of the barite-CMC suspension. The parameters of the power-law model, the mean relative error (MRE) and R-squared are given in Table A-1 (in supplementary material). In the case of polymer

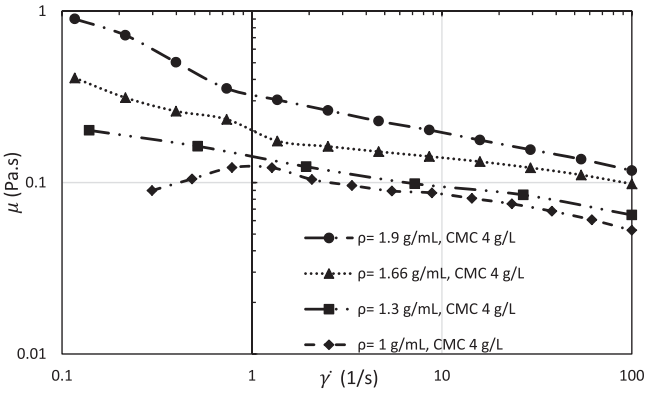

Fig. 4. Rheological behavior of barite-CMC mixtures with different densities.

solution without barite particles a lower R-squared value (corresponding to a worse fit) is due to the shear thickening behavior at very low shear rates.

In addition to power-law model the Carreau fluid model for rheological behavior of the barite-CMC mixtures has been considered (Carreau, 1972). The Carreau model can be expressed as:

$$\mu = \mu_{inf} + \left(\mu_0 - \mu_{inf}\right)\left(1 + (\chi\dot{\gamma})^2\right)^{\frac{l-1}{2}} \tag{23}$$

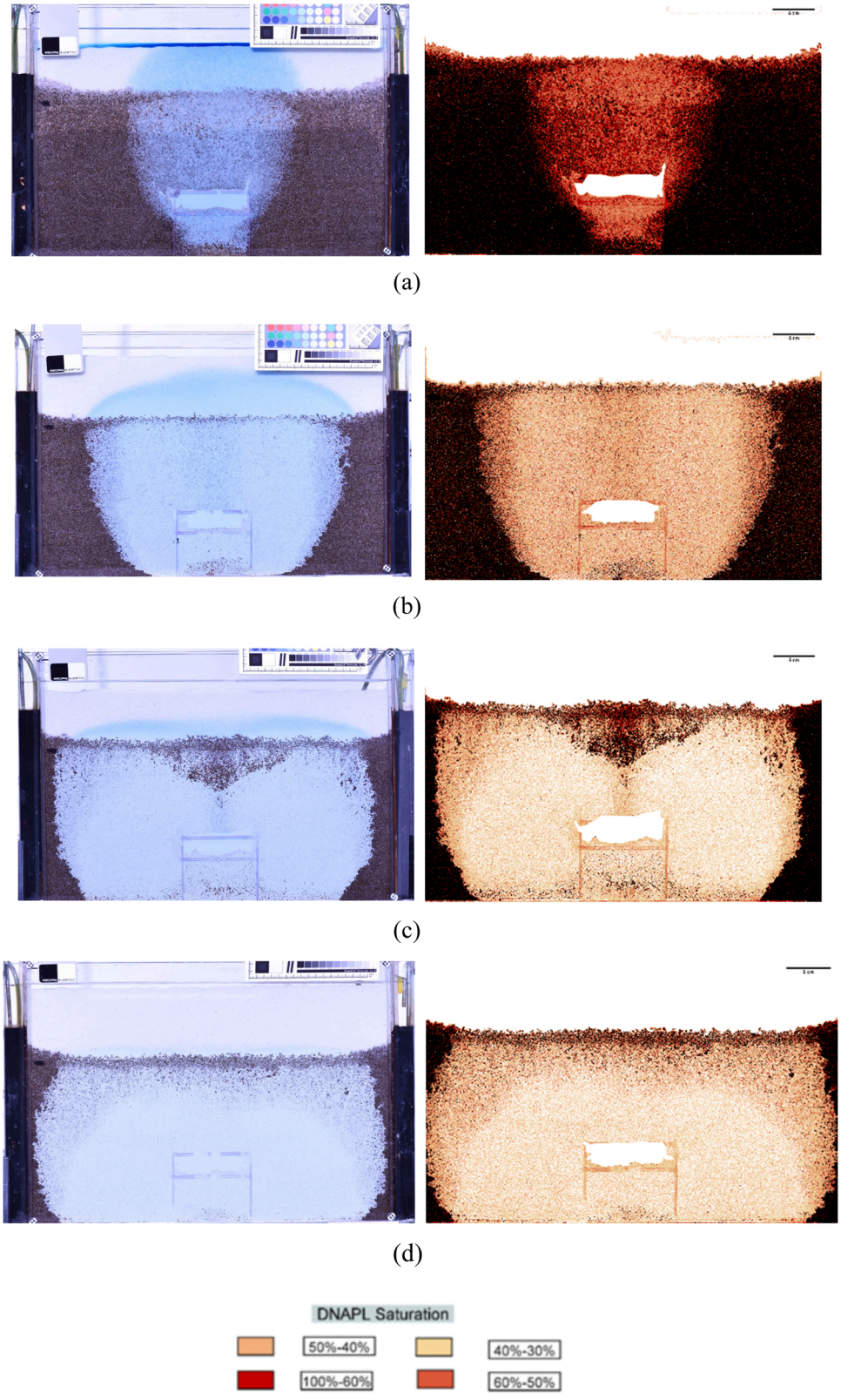

Fig. 5. Comparison of the propagation of the barite-CMC solutions with different densities, the left images are the raw images, and the right images are those interpreted by image analysis. (a) pure polymer injection with density of 1 g/mL, barite-CMC injection with density of (b) 1.3 g/mL, (c) 1.66 g/mL, and (d) 1.9 g/mL.

where, $\mu_0 and \mu_{inf}$ are the viscosities (Pa.s) at zero and infinite shear rate, χ is the relaxation time (s), and l is the power index. The parameters of the Carreau model, and R-squared are given in Table A-2 (in supplementary material). Similar to power-law model for the case of CMC solution without barite particles a lower R-squared value can be seen due to the shear thickening behavior at very low shear rates.

3.2. Experiments on clogging of barite particles in sandpacks

Barite-polymer as a suspension was selected to be injected through the DNAPL saturated zone. The particles suspended in the mixture due to the interaction of several forces can be deposited on the surface of the sand grains. The mass balance analysis of the columns at the end of water postflush after injection of barite-CMC suspensions shows that the mass of retained barite particles for densities of 1.3, 1.66, and 1.9 g/mL were 30.2, 35.5 and 37.3 g, respectively. These quantities of retained barite-particles are quite considerable in comparison to the mass of polymer dissolved in each pore volume of injected suspension (0.5 g). In this regard, the permeability and porosity reductions are mainly attributed to the role of barite particles deposition in sandpacks. In this section, the process of the barite particles clogging in sand for suspensions with different densities is characterized and discussed.

The reduced permeabilities for densities 1.3, 1.66, and 1.9 g/mL are equal to 65, 42, 39.5 Darcy respectively while the initial permeability has been equal to 145 Darcy. Also, The reduced porosities for densities 1.3, 1.66, and 1.9 g/mL are equal to 37.3, 37, 36.9 respectively while the initial porosity has been equal to 39. The degree of clogging for the barite-CMC solution with density of 1.3 g/mL is 0.55 while this value is around 0.71 and 0.73 for densities of 1.66 mL and 1.9 g/mL, respectively. It shows that the capability of the sand grains to retain the barite particles increases by an increase in the concentration of the barite particles in the suspension up to a maximum value. Above this value, there is a weak dependence of deposition of barite particles on the sand grain surfaces on the concentration of the barite in suspension. In addition, the reduction in porosities for various densities of the barite-CMC suspension is in the same trend as the permeability reductions.

3.3. Experimental results of DNAPL displacement using barite-CMC suspension

To compare the efficiency of the injection of polymer mixtures with and without barite on the displacement of the DNAPL, three different densities (1.3 g/mL, 1.66 g/mL, and 1.9 g/mL) of barite-CMC suspension were analyzed. In this regard, several polymer mixtures with different densities were injected into the 2D tank saturated with DNAPL in presence of residual water saturation. During the injection of the invading phase, the level of DNAPL in lateral counter channels (Fig. 1) was kept constant to recover the same amount of DNAPL as the one displaced in the porous medium. Fig. 5 shows the distribution of the polymer and DNAPL (raw and analyzed images) at the end of the experiment, where either there is no more DNAPL production or the invading phase (barite-CMC suspension) has closely approached to the lateral boundaries. For the case of pure polymer injection in the absence of barite particles, the invading phase has a vertical displacement. By increasing the density of polymer mixture using the barite particles, a more lateral displacement of DNAPL is observed, as the buoyancy forces are decreased. In addition, the clogging of barite particles in the pores of the tank has led to density variations in the invading phase. This density variation can be visually seen in the images, where near the front, a zone with a density close to the density of water exists, and behind the front, the density increases up to the density of the invading phase. The results obtained from mass balance data show that the final displacement efficiency $\left(\frac{volume\ of\ DNAPL\ produced}{initial\ volume\ of\ DNAPL\ in\ sand}\right)$ for the case of only CMC solution without particles is around 0.095 while for barite-CMC suspensions with densities of 1.3, 1.66, and 1.9 g/mL, the displacement efficiency is around 0.3, 0.45, and 0.44 respectively.

3.4. Effect of the boundaries on the DNAPL displacement efficiency (closed or open system)

This section is devoted to a comparison between closed and open systems using both experimental and numerical approaches. Concerning the experiments carried out in the 2D tank and analyzed in previous sections, although the displacement efficiency is significantly improved (~4 times more) by increasing the density of the polymer mixture, the displacement efficiency of this technique is still less than that of most other conventional methods (Colombano et al., 2021; Philippe et al., 2020). To have a better understanding, we designed a new experiment in which the top boundaries are closed to avoid vertical displacement and to force the invading fluid to be displaced in the horizontal direction. The barite-CMC suspension with a density of 1.66 g/mL at an injection flow rate equal to 2.8 mL/min was injected into a similar configuration used in the previous experiments in the 2D sandpack with minor differences. More precisely, to have a closed zone of interest with a thickness of 5 cm (instead of 20 cm in previous cases), very fine sand (less than 0.1 mm) was used to block the displacing zone shown in Fig. 6. Figure A-1 (in supplementary material) shows the propagation of the barite-CMC suspension during the displacement in the closed system.

The results showed that the displacement efficiency in the closed system was around 0.88 at the end of the experiment. Some points are of importance to account for this difference: firstly, for the open 2D system, the displacement has been stopped (end of experiment) before reaching the lateral counter channels while in the closed 1D experiment the displacement has been continued to see the invading fluid in the lateral counter channels. Therefore, some parts of the region of interest in the open 2D system are still saturated with DNAPL. Also in comparison to the 1D system, there is a noticeable transition zone in front of fully displaced zone in the 2D system that has a lower DNAPL saturation. Another point that should be noted is that the comparison of the simulation results for both displacements shows that the residual DNAPL saturation in the fully displaced zone for the open 2D system is around 0.34 while in the closed system is around 0.11.

4. Discussion

4.1. Characterization of the clogging of barite particles by finding attachment/detachment parameters

The set of experiments which are explained in Section 3.2 have been carried out to find the dispersivity of barite particles and parameters related to attachment and detachment of barite particles. As it is mentioned in material and methods section, the barite-CMC suspensions were injected at fixed injection rate corresponding to 1 m/day to a fully water saturated column of sand. The effluents of the column were monitored during injection until steady state conditions were reached. The effective diffusion coefficient for the CMC polymer is considered 10^{-11} (m^2/s) which is quite low (Kono, 2014), and the same value is taken into account for barite particles. To find the unknown values including the dispersivity ($\propto$) of barite particles and polymer as well as the attachment and detachment coefficients (θ, β), using an inverse modeling (minimization of the mean squared error), the outlet densities and reduced porosities and permeabilities of the sandpacks from the simulation results were matched with those obtained from the experiment.

It is assumed that the deposited barite particles were retained in their position during water flushing as the hydrodynamic forces of the water were not enough to detach them. In addition, it is considered that the deposition of the barite particles was homogenous along the one-dimensional column and that a maximum concentration of deposited barite particles was reached so that no further deposition on the grain surfaces was possible. To perform the 1D simulations, the appropriate

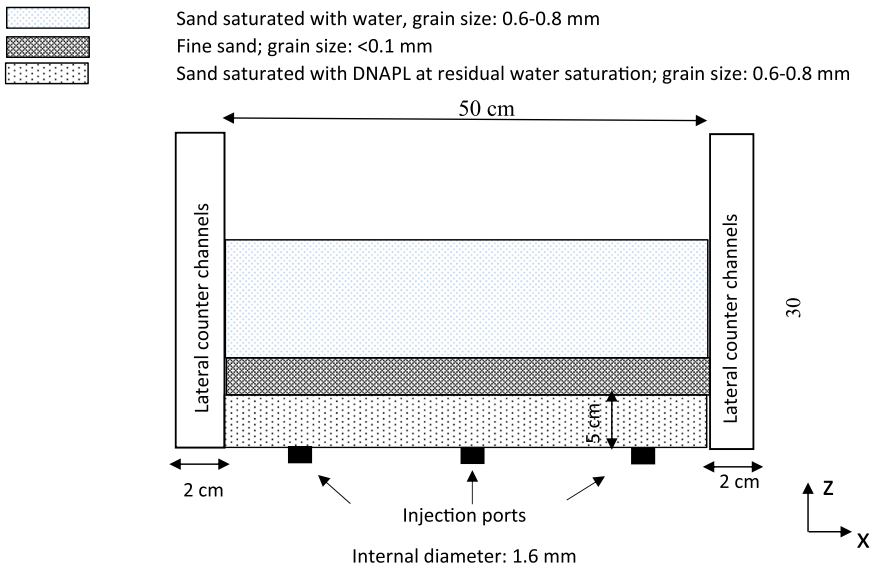

Fig. 6. schematic of configuration and displacement of DNAPL by barite-polymer suspension with the density of 1.66 g/mL in a closed system.

boundary and initial conditions corresponding to the experiments were applied to the domain: constant injection velocity of 1 m/day at the inlet, atmospheric constant pressure at the outlet, and initially fully water saturation inside the sand column. For solute transport the concentration of barite at the inlet is considered in agreement with the densities of barite-CMC suspension while the initial concentration in the column is equal to zero. To match the porosity values, the concentration of barite particles deposited on the sand grain surfaces per unit pore volume (c_s) from simulation was matched with those calculated from reduced porosities at the end of water postflush after barite-CMC injection (Eq. (21)). Then for the reduced permeability values using Carman-Kozeny equation, the correction factors for correlation of porosity and permeability were adjusted. Fig. 7 demonstrates the density curves obtained from the simulations and experiments for different densities of barite-CMC suspensions after breakthrough time. The mean relative error and root mean square error of fitting for all cases are given in Table A-3 (in supplementary material). As it can be seen, the results show that the transition period (between the breakthrough time and the time of the final plateau) for the lighter barite-CMC suspension is longer than for the two other suspensions. This is because the viscosity of denser fluid is higher therefore, a sharper breakthrough curve is observed. The parameters related to the model including the attachment and detachment coefficients and the dispersivities are listed in Table A-3 (in supplementary material).

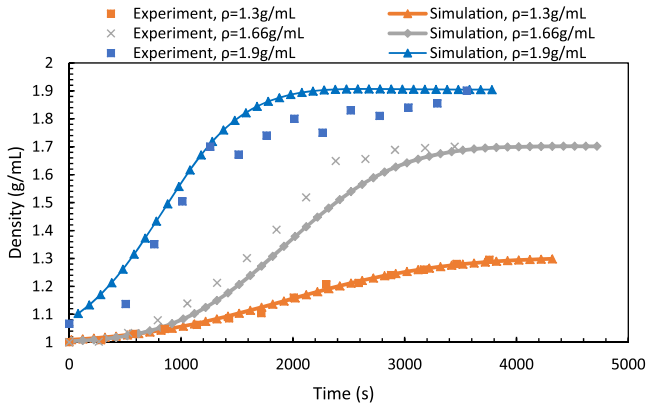

Fig. 7. Comparison between the outlet densities obtained from simulation and experiments after breakthrough time.

4.2. *Numerical simulation results of DNAPL displacement using barite-CMC suspension*

To simulate the process of DNAPL displacement using the barite-CMC suspensions, the clogging process of barite particles was incorporated into the model to include the density variation and permeability/porosity reduction. In this regard, an area on the right-hand side of the two-dimensional system, as shown in Fig. 8, was considered as the representative zone. It is assumed that the flow in high permeable zone near the injection point has been equally distributed in two lateral parts and there is no vertical flow. The schematic of the boundary conditions and geometry of the model is shown in Fig. 8. For the boundaries 3 and 4 as the level of DNAPL has been kept constant during the experiment the constant pressure condition is considered. In these boundaries z (m) is the vertical axis and P_0 is the pressure caused by water height on the top of DNAPL zone. Boundary 3 is a symmetrical boundary condition is considered and for boundaries 2 and 6 no flow condition and for boundary 1 constant injection velocity (1 m/day) are assumed and the constant pressure boundary conditions for boundaries 4 and 5 are considered.

Fig. 9 shows the comparison between the experimental and numerical results. As can be seen, the shape of the invasion fronts of the barite-CMC suspension for various densities obtained by numerical simulation is in agreement with the ones obtained experimentally. As it was mentioned earlier, the large transient zone near the front of the invading phase is attributed to the role of barite-particles clogging and consequently density variation. The higher degree of clogging can also prohibit the backward diffusion of residual DNAPL, which is in favor of the soil remediation purpose.

In Fig. 10, the displacement efficiencies resulting from experiments for various densities of invading phases are compared with those obtained from numerical simulations. The average absolute relative errors $\left(\frac{1}{Nmber\ of\ points}\left|\frac{Displacement\ efficiency_{Exp}-Displacement\ efficiency_{Sim}}{Displacement\ efficiency_{Exp}}\right|\right)$ between the experimental and simulation results are around 0.1, 0.045, 0.083, and 0.158 for densities 1, 1.3, 1.6, and 1.9 g/mL, respectively. The higher error in denser suspensions can be attributed to dependency of saturation functions (capillary pressure and relative permeabilities) on the concentration of barite particles which are clogging in sand. Also, the other reason can be because of the flow above the low permeable layer observed experimentally while we have considered it as an impermeable zone in our model. It is considered that the injected polymer has been completely invaded laterally on two sides of the high permeable zone

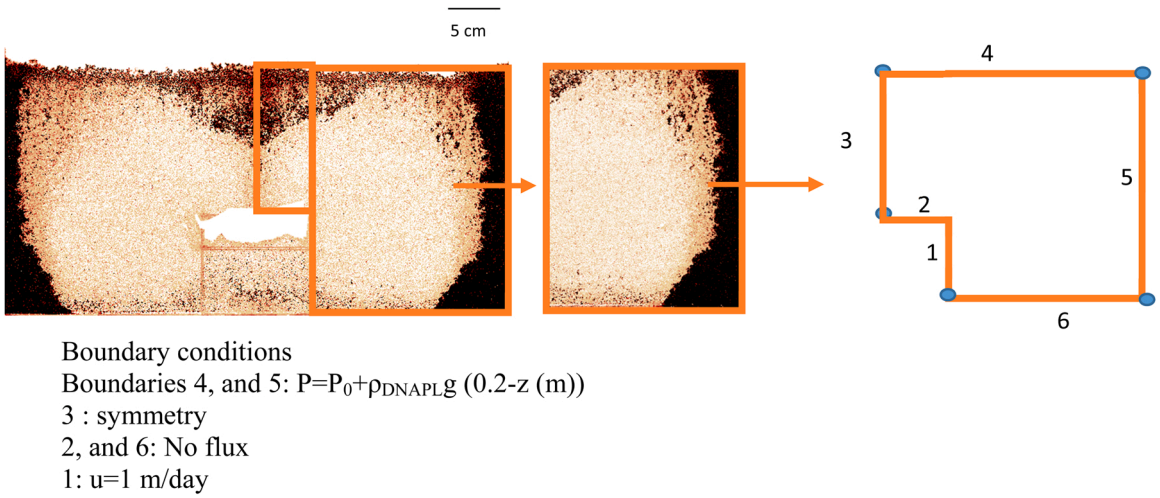

Fig. 8. Geometry used for modeling and the corresponding boundary conditions.

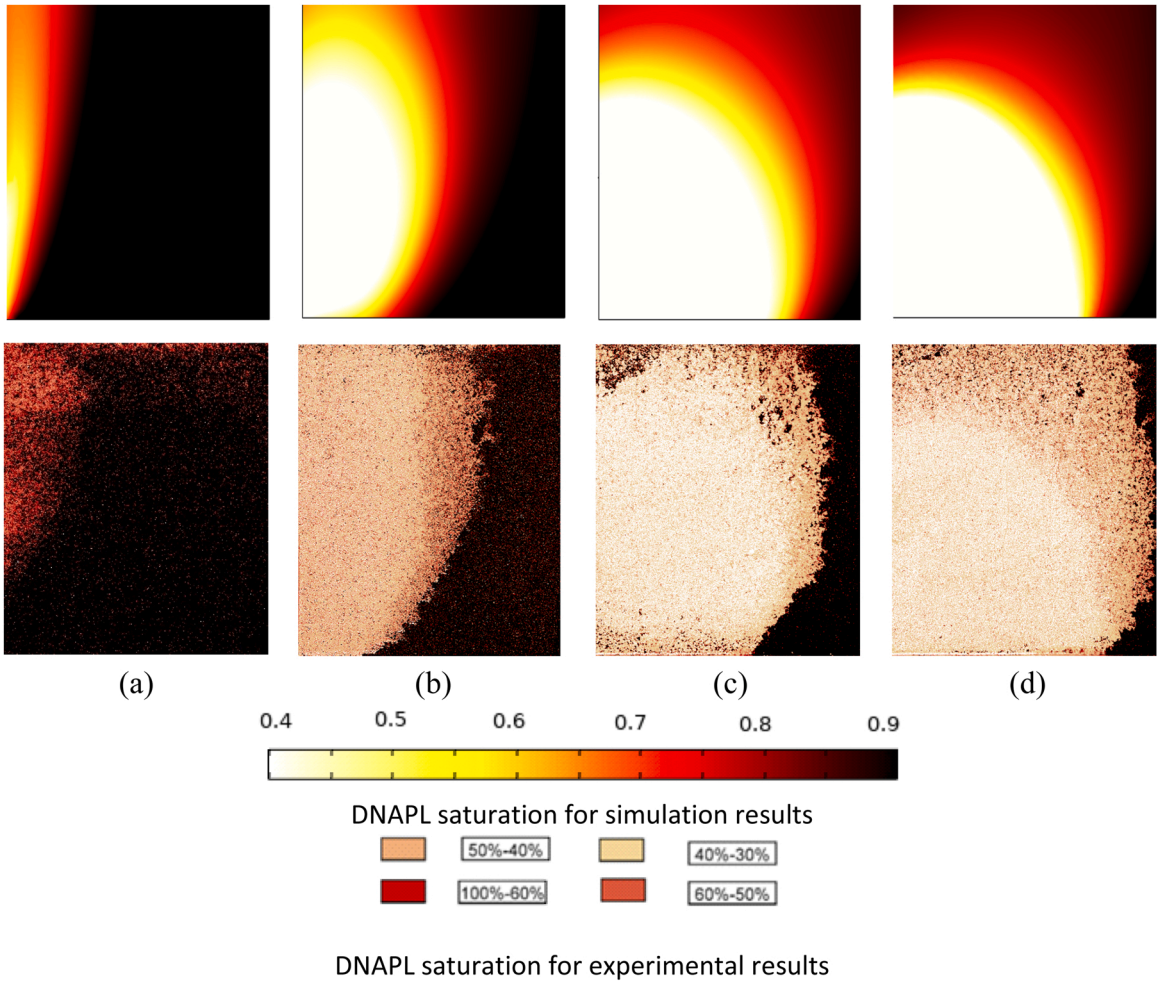

Fig. 9. Comparison between the numerical and experimental results for the end of displacement of DNAPL by barite-CMC suspension, the first row images are from the simulation and the second row images are extracted from the image analysis of experiments. (a) pure polymer injection with density of 1 g/mL after 94 min, barite-CMC injection with density of (b) 1.3 g/mL after 234 min, (c) 1.66 g/mL after 240 min, and (d) 1.9 g/mL after 220 min.

and no vertical displacement takes place from low permeable zone.

4.3. Analysis of the transition zone in displaced zone

During the injection of the barite-CMC suspension into the DNAPL saturated zone, due to the deposition of the barite particles onto the sand

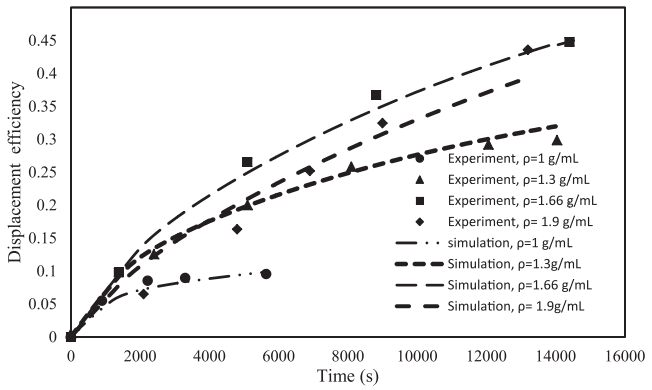

Fig. 10. Comparison between the experimental displacement efficiencies for various densities of invading phases (obtained using mass balance) and those obtained from simulation results.

grain surfaces, and also the mixing with the residual water saturation inside the DNAPL saturated zone, a zone inside the displaced zone near the front has been formed with densities less than the density of invading barite-CMC suspension. Then due to the buoyancy forces, the lighter region has formed a transition zone in front of the fully displaced zone. This transition zone has grown to reach the water zone above the DNAPL saturated zone. To elucidate the diffusive behavior of the segregated fluid from the invading barite-CMC suspension, the evolution of the transition zone, as well as the fully displaced zone (Figure A-2), were analyzed.

The ratio of the transition zone (A_t) to the area of the fully displaced zone (A_d) versus the ratio of the area of the total displaced zone (transition and fully displaced zones, ($A_t + A_d$)) to the surface area of the region of interest (A_r) is plotted in Figure A-3. At the beginning of the injection, A_t/A_d is at maximum, and then it decreases. In other words, as the front of transition zones reaches the layer of water above the region of interest the transition zone propagation is deaccelerated. Furthermore, the higher the density of barite-CMC suspension (i.e. higher density difference between the invading fluid and water), the higher is the ratio of A_t/A_d. For example, when half of the region of interest is covered by the invading fluid ($(A_t + A_d)/A_r = 0.5$), A_t/A_d is around 1.38, 0.91, and 0.61 for densities of 1.9, 1.66, and 1.3 g/mL, respectively.

As it was shown in Figure A-2 (in supplementary material), since the beginning of the injection of barite-CMC suspension into the tank, a transition zone was formed in the front of fully displaced zone and it was moving vertically as a sign for a density driven flow. Several factors can influence the transition zone in porous media. In the case of barite-CMC, the deposition and dispersion of barite particles can impact the transition zone.

4.4. Difference between closed and open systems

There are several studies in which the role of various parameters including boundaries on residual oil saturation, relative permeability and capillary pressure has been investigated (Ataie-Ashtiani et al., 2002; Hollenbeck and Jensen, 1998; Xu et al., 2016; Alamooti et al., 2018). Hollenbeck and Jensen (1998) did several experiments in a vertical column which was homogenously packed with sand. Various initial capillary pressure heads (from 11.5 to 83.5 cm) have been used. Their results showed that the higher the capillary pressure head, the higher the capillary pressure-saturation curve would lie. Ataie-Ashtiani et al. (2002) by means of numerical experiments investigated the combined effects of boundary conditions and heterogeneity on capillary pressure and relative permeability. They found that these saturation functions are strongly influenced by heterogeneities and boundary conditions. Xu et al. (2016) did several imbibition experiments at core scale to evaluate the role of displacement pressure gradient on relative permeability curves. They found that at higher displacement pressure gradients the residual oil saturation decreases, the water relative permeability lies higher and oil relative permeability moves to the right. In this regard to match the same production history, residual oil saturation and saturation profile in the closed system, the parameters of capillary pressure and relative permeability curves were redetermined. As a result, the capillary pressure curve lies higher in the case of a closed system in comparison to the open one. For the relative permeabilities when the system is closed the oil and water relative permeability curves have moved to the right.

This ignorance of the difference between the residual saturations in closed and open systems can lead to an overestimation of displacement efficiency in real field. Thus, it is highly recommended to consider the role of the upper boundary while designing soil remediation methods at the field scale. A way to avoid this problem in real sites could be using a blocking agent to block the upper part of the DANPL contaminated zone to increase the efficiency of the displacement.

5. Conclusions

In this study, using two-dimensional tank experiments and corresponding numerical modeling of the displacement process in porous media, the efficiency of the injection of densified polymer suspensions on the displacement of DNAPL was investigated. It was shown that adding barite particles to densify the polymer solution could improve the displacement efficiency of DNAPL more than 4 times. Using one-dimensional column experiments, it was demonstrated that the barite-CMC suspensions can cause a permeability reduction equal to 55%, 70%, and 72% for different suspensions with densities of 1.3, 1.66, and 1.9 g/mL, respectively. Moreover, the presence of barite particles can result in a higher viscosity of the polymer suspension while keeping a similar rheological behavior. It was shown that for a confined system which is not a good representative of real polluted site, a higher unrealistic displacement efficiency can be obtained. The DNAPL displacement by barite-CMC solution was numerically simulated using generalized Darcy's law and the continuity equation. In addition, the clogging of the porous medium by the suspended barite particles was modeled using the transport equation of diluted species. A very good qualitative agreement between the experimental saturation fields and the simulated ones was observed.

CRediT authorship contribution statement

Amir Alamooti: Methodology, Conceptualization, Visualization, Writing – original draft. **Stéfan Colombano**: Conceptualization, Supervision, Funding acquisition, Project administration, Writing – review & editing. **Sagyn Omirbekov**: Methodology, Conceptualization, Validation. **Azita Ahmadi**: Supervision, Validation, Writing – review & editing. **Fabien lion**: Resources, Visualization. **Hossein Davarzani**: Supervision, Writing – review & editing, Visualization.

Environmental Implication

Chlorinated DNAPL spills are frequent and due to their high toxicity they can negatively influence the soil and groundwater quality by penetrating through the soil and forming insoluble lenses. This study discusses a novel in situ remediation technique by introducing the densified polymer suspension for displacement of DNAPL from the contaminated zone. The experiments have been done on an unconfined system instead of an idealistic one to represent the real polluted site. This environmentally friendly method can effectively improve the recovery of DNAPL by overcoming the buoyancy forces caused by high density of the chlorinated compounds.

Declaration of Competing Interest

The authors declare that they have no known competing financial interests or personal relationships that could have appeared to influence the work reported in this paper.

Data availability

No data was used for the research described in the article.

Acknowledgments

This study was performed as part of the PAPIRUS project. The authors would like to thank ADEME (French Environment and Energy Management Agency) for co-funding the project under the "GESIPOL" program and BRGM/DEPA and ADEME for providing the PhD grant for Amir Alamooti. The authors also gratefully acknowledge the financial support provided to the PIVOTS project by the "Région Centre – Val de Loire" and the European Regional Development Fund. We thank INOVYN for the assistance provided during the PAPIRUS project, in particular for providing access to the Tavaux site.

Appendix A. Supporting information

Supplementary data associated with this article can be found in the online version at doi:10.1016/j.jhazmat.2022.129702.

References

Alamooti, A.H.M., Azizi, Q., Davarzani, H., 2020. Direct numerical simulation of trapped-phase recirculation at low capillary number. Adv. Water Resour. 145, 103717 https://doi.org/10.1016/j.advwatres.2020.103717.

Alamooti, A.M., Ghazanfari, M.H., Masihi, M., 2018. Investigating the relative permeability behavior in presence of capillary effects in composite core systems. J. Pet. Sci. Eng. 160, 341–350. https://doi.org/10.1016/j.petrol.2017.10.051.

Alamooti, A.M., Malekabadi, F.K., 2018. An introduction to enhanced oil recovery. In: Fundamentals of Enhanced Oil and Gas Recovery from Conventional and Unconventional Reservoirs. Elsevier Inc, pp. 1–40. https://doi.org/10.1016/B978-0-12-813027-8.00001-1.

Ardakani, A.G., Mohammadi Alamooti, A.H., Rasaei, M.R., Javadi, A., Ghazanfari, M.H., Davarzani, H., 2020. Monitoring polymer-enhanced foam displacements through heterogeneous porous media: a pore-scale study. J. Energy Resour. Technol. 142 https://doi.org/10.1115/1.4046943.

Ataie-Ashtiani, B., Hassanizadeh, S.M., Celia, M.A., 2002. Effects of heterogeneities on capillary pressure–saturation–relative permeability relationships. J. Contam. Hydrol. 56, 175–192.

Auset, M., Keller, A.A., 2004. Pore-scale processes that control dispersion of colloids in saturated porous media. Water Resour. Res. 40 https://doi.org/10.1029/2003WR002800.

Bear, J., 2013, Dynamics of fluids in porous media. Courier Corporation.

Bedrikovetsky, P., Zeinijahromi, A., Siqueira, F.D., Furtado, C.A., de Souza, A.L.S., 2012. Particle detachment under velocity alternation during suspension transport in porous media. Transp. Porous Media 91, 173–197. https://doi.org/10.1007/s11242-011-9839-1.

Benchabane, A., Bekkour, K., 2008. Rheological properties of carboxymethyl cellulose (CMC) solutions. Colloid Polym. Sci. 286, 1173–1180. https://doi.org/10.1007/S00396-008-1882-2/FIGURES/5.

Bern, P.A., Zamora, M., Slater, K.S., Hearn, P.J., 1996, The influence of drilling variables on barite sag, in: SPE Annual Technical Conference and Exhibition. OnePetro.

Boek, E.S., Hall, C., Tardy, P.M.J., 2012. Deep bed filtration modelling of formation damage due to particulate invasion from drilling fluids. Transp. Porous Media 91, 479–508. https://doi.org/10.1007/s11242-011-9856-0.

Brooks, R.H., Corey, A.T., 1964. Hydraulic properties of porous media and their relation to drainage design. Trans. ASAE 7, 26–28.

Carreau, P.J., 1972. Rheological equations from molecular network theories. Trans. Soc. Rheol. 16, 99–127.

Chauveteau, G., Zaitoun, A., 1981, Basic rheological behavior of xanthan polysaccharide solutions in porous media: effects of pore size and polymer concentration, in: Proceedings of the First European Symposium on Enhanced Oil Recovery, Bournemouth, England, Society of Petroleum Engineers, Richardson, TX. pp. 197–212.

Colombano, S., Davarzani, H., van Hullebusch, E.D., Huguenot, D., Guyonnet, D., Deparis, J., Ignatiadis, I., 2020. Thermal and chemical enhanced recovery of heavy chlorinated organic compounds in saturated porous media: 1D cell drainage-imbibition experiments. Sci. Total Environ. 706, 135758 https://doi.org/10.1016/j.scitotenv.2019.135758.

Colombano, S., Davarzani, H., van Hullebusch, E.D., Huguenot, D., Guyonnet, D., Deparis, J., Lion, F., Ignatiadis, I., 2021. Comparison of thermal and chemical enhanced recovery of DNAPL in saturated porous media: 2D tank pumping experiments and two-phase flow modelling. Sci. Total Environ. 760, 143958 https://doi.org/10.1016/j.scitotenv.2020.143958.

Darby, Ronald, Darby, Ron, Chhabra, R.P., 2017. Chemical Engineering Fluid Mechanics, Revised and Expanded. CRC Press.

Davarzani, H., Aranda, R., Colombano, S., Laurent, F., Bertin, H., 2021. Experimental study of foam propagation and stability in highly permeable porous media under lateral water flow: Diverting groundwater for application to soil remediation. J. Contam. Hydrol. 243, 103917 https://doi.org/10.1016/J.JCONHYD.2021.103917.

De Vries, J., 1972. Soil filtration of wastewater effluent and the mechanism of pore clogging. J. (Water Pollut. Control Fed. 565–573.

Dejam, M., Hassanzadeh, H., Chen, Z., 2014. Reinfiltration through liquid bridges formed between two matrix blocks in fractured rocks. J. Hydrol. 519, 3520–3530. https://doi.org/10.1016/j.jhydrol.2014.10.050.

Duffield, A.R., Ramamurthy, R.S., Campanelli, J.R., 2003. Surfactant enhanced mobilization of mineral oil within porous media. Water Air. Soil Pollut. 143, 111–122. https://doi.org/10.1023/A:1022829204883.

Flores, G., Katsumi, T., Inui, T., Kamon, M., 2011. A simplified image analysis method to study LNAPL migration in porous media. Soils Found. 51, 835–847.

Hanson, P.M., Trigg, T.K., Rachal, G., Zamora, M., 1990, Investigation of barite sag in weighted drilling fluids in highly deviated wells, in: SPE Annual Technical Conference and Exhibition. OnePetro.

Herzig, J.P., Leclerc, D.M., Le Goff, P.L., 1970. Flow of suspensions through porous media— application to deep filtratio. Ind. Eng. Chem. 62, 8–35. https://doi.org/10.1021/ie50725a003.

Hollenbeck, K.-J., Jensen, K.H., 1998. Experimental evidence of randomness and nonuniqueness in unsaturated outflow experiments designed for hydraulic parameter estimation. Water Resour. Res. 34, 595–602.

Hommel, J., Coltman, E., Class, H., 2018. Porosity–permeability relations for evolving pore space: a review with a focus on (bio-)geochemically altered porous media. Transp. Porous Media. https://doi.org/10.1007/s11242-018-1086-2.

Jeong, S.W., 2005. Evaluation of the use of capillary numbers for quantifying the removal of DNAPL trapped in a porous medium by surfactant and surfactant foam floods. J. Colloid Interface Sci. 282, 182–187. https://doi.org/10.1016/j.jcis.2004.08.108.

Johnson, J.C., Sun, S., Jaffé, P.R., 1999. Surfactant enhanced perchloroethylene dissolution in porous media: the effect on mass transfer rate coefficients. Environ. Sci. Technol. 33, 1286–1292. https://doi.org/10.1021/ES980908D.

Kilbane, J.J., Chowdiah, P., Kayser, K.J., Misra, B., Jackowski, K.A., Srivastava, V.J., Sethu, G.N., Nikolov, A.D., Wasan, D.T., Hayes, T.D., 1997. Remediation of contaminated soils using foams. L. Contam. Reclam. 5, 41–54.

Kono, H., 2014. Characterization and properties of carboxymethyl cellulose hydrogels crosslinked by polyethylene glycol. Carbohydr. Polym. 106, 84–93. https://doi.org/10.1016/j.carbpol.2014.02.020.

Langwaldt, J.H., Puhakka, J.A., 2000. On-site biological remediation of contaminated groundwater: A review. In: Environmental Pollution. Elsevier, pp. 187–197. https://doi.org/10.1016/S0269-7491(99)00137-2.

Li, Y., Abriola, L.M., Phelan, T.J., Ramsburg, C.A., Pennell, K.D., 2007. Experimental and numerical validation of the total trapping number for prediction of DNAPL mobilization. Environ. Sci. Technol. 41, 8135–8141. https://doi.org/10.1021/es070834i.

Littmann, W., 1988. Polymer Flooding. Elsevier.

Liu, S., 2008, Alkaline Surfactant Polymer enhanced oil recovery process. Rice University.

Liu, W.H., Yu, T.L., Lin, H.L., 2007. Shear thickening behavior of dilute poly(diallyl dimethyl ammonium chloride) aqueous solutions. Polym. (Guildf.) 48, 4152–4165. https://doi.org/10.1016/J.POLYMER.2007.05.012.

Martel, K.E., Martel, R., Lefebvre, R., Gélinas, P.J., 1998. Laboratory study of polymer solutions used for mobility control during in situ NAPL recovery. Gr. Water Monit. Remediat. 18, 103–113. https://doi.org/10.1111/j.1745-6592.1998.tb00734.x.

Martel, R., Hébert, A., Lefebvre, R., Gélinas, P., Gabriel, U., 2004. Displacement and sweep efficiencies in a DNAPL recovery test using micellar and polymer solutions injected in a five-spot pattern. J. Contam. Hydrol. 75, 1–29. https://doi.org/10.1016/j.jconhyd.2004.03.007.

Mashayekhizadeh, V., Ghazanfari, M.H., Kharrat, R., Dejam, M., 2011. Pore-level observation of free gravity drainage of oil in fractured porous media. Transp. Porous Media 87, 561–584. https://doi.org/10.1007/s11242-010-9701-x.

McCarty, P.L., 2010. Groundwater Contamination by Chlorinated Solvents: History, Remediation Technologies and Strategies. Springer, New York, NY, pp. 1–28. https://doi.org/10.1007/978-1-4419-1401-9_1.

Merian, E., Anke, M., Ihnat, M., Stoeppler, M., 2004. Elements and their Compounds in the Environment: Occurrence, Analysis and Biological Relevance. Wiley-VCH Verlag GmbH & Co. KGaA,.

Miller, C.T., Hill, E.H., Moutier, M., 2000. Remediation of DNAPL-contaminated subsurface systems using density-motivated mobilization. Environ. Sci. Technol. 34, 719–724.

O'Carroll, D., Sleep, B., Krol, M., Boparai, H., Kocur, C., 2013. Nanoscale zero valent iron and bimetallic particles for contaminated site remediation. Adv. Water Resour. 51, 104–122. https://doi.org/10.1016/J.ADVWATRES.2012.02.005.

Omirbekov, S., Davarzani, H., Colombano, S., Ahmadi-Senichault, A., 2020. Experimental and numerical upscaling of foam flow in highly permeable porous media. Adv. Water Resour. 146, 103761 https://doi.org/10.1016/j.advwatres.2020.103761.

Pennell, K.D., Pope, G.A., Abriola, L.M., 1996. Influence of viscous and buoyancy forces on the mobilization of residual tetrachloroethylene during surfactant flushing. Environ. Sci. Technol. 30, 1328–1335. https://doi.org/10.1021/es9505311.

Pérez Paricio, A., 2001, Integrated modelling of clogging processes in artificial groundwater recharge. Universidad Politécnica de Cataluña.

Philippe, N., Davarzani, H., Colombano, S., Dierick, M., Klein, P.Y., Marcoux, M., 2020. Experimental study of the temperature effect on two-phase flow properties in highly permeable porous media: Application to the remediation of dense non-aqueous phase liquids (DNAPLs) in polluted soil. Adv. Water Resour. 146, 103783 https://doi.org/10.1016/j.advwatres.2020.103783.

Ropp, R.C., 2012. Encyclopedia of the Alkaline Earth Compounds. Newnes.

Roy, J.W., Smith, J.E., Gillham, R.W., 2004. Laboratory evidence of natural remobilization of multicomponent DNAPL pools due to dissolution. J. Contam. Hydrol. 74, 145–161. https://doi.org/10.1016/j.jconhyd.2004.02.009.

Sandiford, B.B., 1964. Laboratory and field studies of water floods using polymer solutions to increase oil recoveries. J. Pet. Technol. 16, 917–922.

Schincariol, R.A., Herderick, E.E., Schwartz, F.W., 1993. On the application of image analysis to determine concentration distributions in laboratory experiments. J. Contam. Hydrol. 12, 197–215.

Schulz, K.J., DeYoung, J.H., Seal, R.R., Bradley, D.C., 2018, Critical mineral resources of the United States: economic and environmental geology and prospects for future supply. Geological Survey.

Silva, J.A.K., Liberatore, M., Mccray, J.E., Asce, M., 2013, Characterization of Bulk Fluid and Transport Properties for Simulating Polymer-Improved Aquifer Remediation. ⟨https://doi.org/10.1061/(ASCE)EE.1943–7870.0000616⟩.

Smith, M.M., Silva, J.A.K., Munakata-Marr, J., Mccray, J.E., 2008. Compatibility of polymers and chemical oxidants for enhanced groundwater remediation. Environ. Sci. Technol. 42, 9296–9301. https://doi.org/10.1021/es800757g.

Stroo, H.F., Leeson, A., Marqusee, J.A., Johnson, P.C., Ward, C.H., Kavanaugh, M.C., Sale, T.C., Newell, C.J., Pennell, K.D., Lebrón, C.A., Unger, M., 2012. Chlorinated ethene source remediation: Lessons learned. Environ. Sci. Technol. https://doi.org/10.1021/es204714w.

Tsakiroglou, C.D., Sikinioti-Lock, A., Terzi, K., Theodoropoulou, M., 2018. A numerical model to simulate the NAPL source zone remediation by injecting zero-valent iron nanoparticles. Chem. Eng. Sci. 192, 391–413. https://doi.org/10.1016/J.CES.2018.07.037.

Vigneswaran, S., Suazo, R.B., 1987. A detailed investigation of physical and biological clogging during artificial recharge. Water Air. Soil Pollut. 35, 119–140. https://doi.org/10.1007/BF00183848.

Voronov, R., VanGordon, S., Sikavitsas, V.I., Papavassiliou, D.V., 2010. Computational modeling of flow-induced shear stresses within 3D salt-leached porous scaffolds imaged via micro-CT. J. Biomech. 43, 1279–1286. https://doi.org/10.1016/j.jbiomech.2010.01.007.

Wang, S., Mulligan, C.N., 2004. An evaluation of surfactant foam technology in remediation of contaminated soil. Chemosphere 57, 1079–1089.

Xu, J., Guo, C., Jiang, R., Wei, M., 2016. Study on relative permeability characteristics affected by displacement pressure gradient: Experimental study and numerical simulation. Fuel 163, 314–323. https://doi.org/10.1016/J.FUEL.2015.09.049.

Yuan, H., Shapiro, A.A., 2011. A mathematical model for non-monotonic deposition profiles in deep bed filtration systems. Chem. Eng. J. 166, 105–115. https://doi.org/10.1016/j.cej.2010.10.036.

Zamani, A., Maini, B., 2009. Flow of dispersed particles through porous media - Deep bed filtration. J. Pet. Sci. Eng. 69, 71–88. https://doi.org/10.1016/j.petrol.2009.06.016.

Zhang, Z.F., Smith, J.E., 2002. Visualization of DNAPL fingering processes and mechanisms in water-saturated porous media. Transp. Porous Media 48, 41–59. https://doi.org/10.1023/A:1015675404195.

Zheng, X.L., Shan, B.B., Chen, L., Sun, Y.W., Zhang, S.H., 2014. Attachment-detachment dynamics of suspended particle in porous media: Experiment and modeling. J. Hydrol. 511, 199–204. https://doi.org/10.1016/j.jhydrol.2014.01.039.

Zhong, L., Oostrom, M., Truex, M.J., Vermeul, V.R., Szecsody, J.E., 2013. Rheological behavior of xanthan gum solution related to shear thinning fluid delivery for subsurface remediation. J. Hazard. Mater. 244–245, 160–170. https://doi.org/10.1016/J.JHAZMAT.2012.11.028.